Improved accuracy of micro PIV measurement using image overlapping technique

Chuong V. Nguyen[1*], Andreas Fouras[2], Josie Carberry[1+]

1: Fluids Laboratory for Aeronautical and Industrial Research (FLAIR),
Department of Mechanical Engineering, Monash University, VIC 3800, Australia
* Chuong.Nguyen@eng.monash.edu.au
+ Josie.Carberry@eng.monash.edu.au
2: Division of Biomedical Engineering, Monash University, VIC 3800, Australia
Fouras@eng.monash.edu

Abstract In micro PIV, volume illumination allows particles within an image depth to contribute to the correlation and the measurement is a weighted average of the flow within the depth of correlation. For relatively large correlation depths, this may result in distortion of the correlation peak and significant measurement errors. It is therefore desirable to reduce the effect of the depth of correlation. We present an image overlapping technique which effectively reduces the effect of the depth of correlation by reducing the non-dimensional depth of measurement z*. Investigations performed on both synthetic and experimental images show that image overlapping can effectively improve the measurement accuracy both by reducing z* and by increasing signal-to-noise ratio. These improvements are particularly important for measurements of boundary flows where velocity gradients are large. Furthermore, for low numerical aperture lenses, image overlapping can produce successful micro PIV measurement of boundary flows where other techniques fail to produce accurate results.

1. Introduction

Micro particle image velocimetry (micro PIV) is an extension of PIV to measure flows at the micro scale. Meinhart *et al* (1999) first described a micro PIV system consisting of a microscope connected to a camera and using fluorescent particles as flow tracers. Due to the small measuring region, it is impossible to create a laser sheet to capture a slice of the flow, as traditionally done in macro PIV. Instead the laser beam illuminates all particles within the viewing volume, both in-focus and out-of-focus particles appear in the image.

PIV measurement relies on correlations between consecutive images to determine flow velocities. Thus the accurate detection of the correlation peaks is vital. The depth of correlation z_{corr} is defined firstly by Werely *et al* (1999) as the image depth over which particles can affect significantly the image correlation and therefore the measurement result. The correlation depth has been described as a function of the lens properties according to the theoretical relationship (Bourdon *et al* 2006, Olson and Adrian 2000):

$$z_{corr} = \left[\frac{\left(1-\sqrt{\varepsilon}\right)}{\sqrt{\varepsilon}} \left(\frac{n_0^2 d_p^2}{4NA^2} + \frac{5.95(M+1)^2 \lambda^2 n_0^4}{16M^2 NA^4} \right) \right]^{1/2} \quad (1)$$

where:

ε: threshold weighting function value

n_0: refractive index of immersion medium ($n_0 = 1$ for air)

d_p: particle diameter

NA: lens numerical aperture

M: lens magnification

λ: wavelength of fluorescent light emitted from particles

Olson and Adrian (2000) recommended that the depth of correlation extends to the point where particle intensity drops below 1% of the intensity at the focal plane, .i.e. $\varepsilon = 0.01$. This choice of ε means that:

$$z_{corr} \approx 3\sigma_{corr} \tag{2}$$

where σ_{corr} is one standard deviation of the Gaussian distribution of the particle correlation weighting function in z direction.

The velocity calculated from the correlation peak is a weighted average over the depth of focus. In regions of high velocity gradient, this can result in significant errors. These measurement errors can be reduced by decreasing the depth of correlation. As described in equation (1) the depth of correlation depends on optical properties, such as the numerical aperture and lens magnification, and particle diameter. The depth of correlation can also be altered by image processing. Bourdon *et al* (2004) proposed a power-filter method to modify the depth of correlation in micro PIV by raising the image intensity to a chosen power. Their method can reduce or increase the effective depth of correlation by a factor of up to 2. In this paper we present an alternative method to reduce the effect of depth of correlation by applying image overlapping. Our method can reduce the effect of the depth of measurement by up to a factor of 3.

Depth of correlation and measurement accuracy

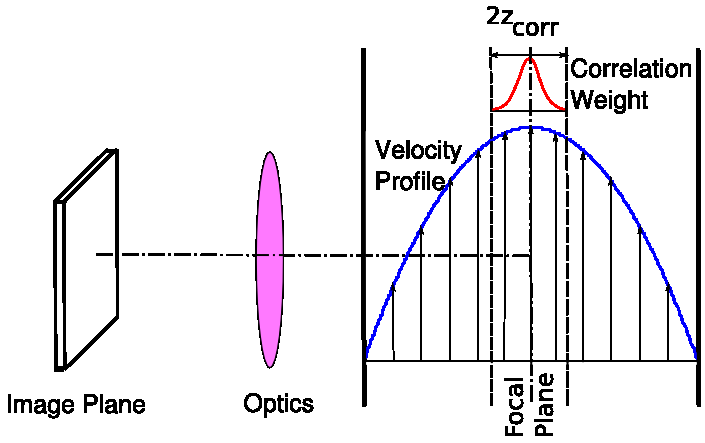

Fig. 1 Schematic showing the optical setup for micro PIV of channel flow. The focal plane is shown at the center of the channel with an associated depth of correlation and particle correlation weighting function.

Fig. 1 shows a flow example demonstrating the depth of correlation with Gaussian weighting distribution around the focal plane, where the focal plane is at the center of a parabolic velocity profile. Moving particles within the depth of correlation are captured onto the image plane and therefore contribute to the measurement of the velocity profile. The depth of correlation has the effect of applying a low-pass filter to the measurement; thus for the parabolic velocity profile shown in Fig. 1, the velocity will be under-estimated at the center and over-estimated at the wall. Increasing the depth of correlation increases the magnitude of these measurement errors as illustrated in Fig. 2a,b. For the same depth of correlation, the percentage of error is greatest near the wall. Thus, the depth of correlation can significantly reduce the accuracy of micro PIV measurements of wall shear gradient.

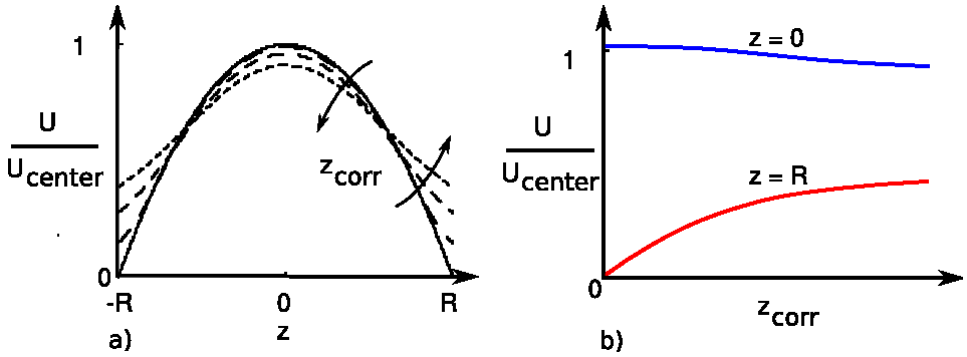

Fig. 2 Effect of increasing the depth of correlation, z_{corr}, on the measurement of a parabolic velocity profile. **a)** Normalized measured velocity profiles within the flow depth. The solid line is the true profile. The dashed lines are the velocity profiles measured with a finite z_{corr} where the arrows indicate the affect of increasing z_{corr}. **b)** Change in the velocity measurement at the center plane (z = 0) and at the wall (z = R) as a function of z_{corr}.

2. Image overlapping technique

Image overlapping was introduced by Wereley *et al* (2002) to increase particle density in PIV images and the number of valid velocity vectors in regions of low particle-seeding density. Image overlapping produces a maximal image from a set of images, where each pixel in the final image is the maximal value from the image set at that pixel position. When image overlapping is applied to micro PIV images an additional effect of image overlapping has been discovered. On average, the brightest particles in the image are in-focus, while the weaker particles are typically out-of-focus. By applying image overlapping, the brighter particles are selected and they dominate the resulting image, thereby reducing the effects of out-of-focus particles and the depth of correlation. By reducing the effect of the depth of correlation, the accuracy of the measurement is increased. Image overlapping technique can be used with correlation averaging (Wereley *et al* 2002) to provide optimal results. A disadvantage of image overlapping is that the shape of the particles is distorted when they are close to one another. This can be considered as loss of information and excessive image overlapping can introduce errors. Image overlapping is also a time-averaging technique.

Image overlapping is performed on a set of N image pairs I and I′ to obtain time averaged velocity measurements as follows. The set of image pairs are divided into M subsets. A maximal function is applied to each subset to produce a single overlapped image pair. The number of images in the subset is defined as the overlap number N_{ov}, thus:

$$N_{ov} = N/M \tag{3}$$

$$I_{ov}(x, y) = \max\{I_i(x, y),\ i = 1{:}N_{ov}\} \tag{4a}$$

$$I'_{ov}(x, y) = \max\{I'_i(x, y),\ i = 1{:}N_{ov}\} \tag{4b}$$

Cross correlation is then applied to the overlapped image pair. As N_{ov} varies from 1 (no image overlapping) to N, M varies from N to 1. For M>1, correlation maps from M overlapped image pairs are averaged into a single map.

As N_{ov} varies, the shape and center of the resulting correlation peak changes, as so does the resulting velocity. Fig. 3 summarizes the image overlapping process and the effects of increasing N_{ov} on the correlation peak and velocity measurement at the center plane of the parabolic flow shown previously in Fig. 2. Without image overlapping, the correlation peak is distorted by out-of-focus particles where the velocities of the out-of-focus particles are less than the velocity at the center plane U_{center}. This produces a wide asymmetrical correlation peak. With increasing image overlapping, the correlation peak becomes narrower, and the distortion is reduced with the center of the peak moving towards the true value of U_{center}.

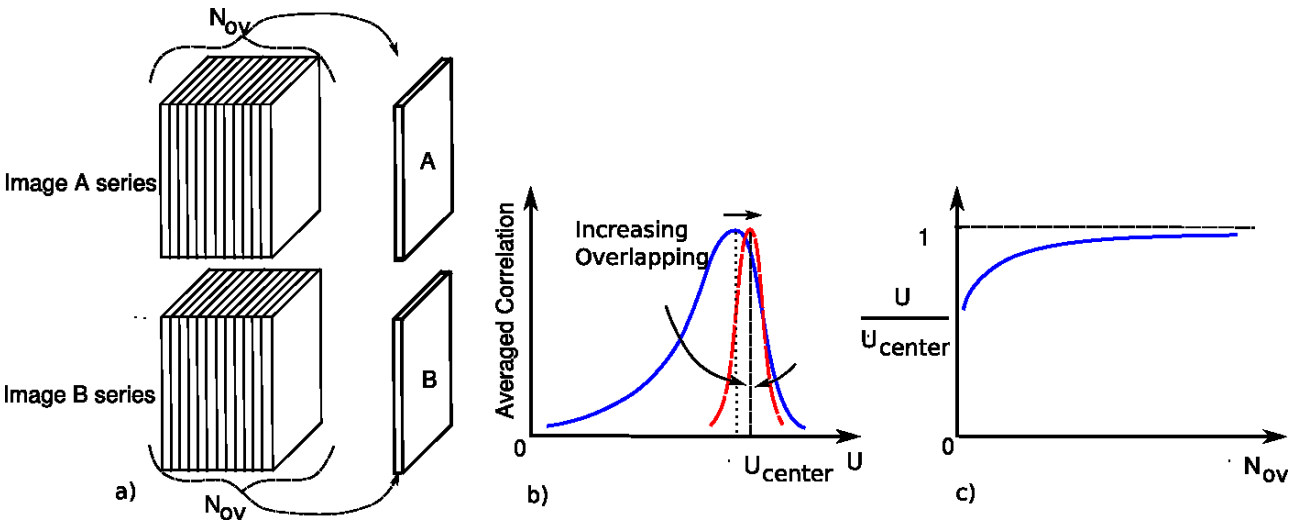

Fig. 3 The effect of image overlapping on the cross correlation peak and the velocity measurement at the center of a parabolic flow profile. **a)** Image series of the first and second exposures are overlapped. **b)** The correlation peak becomes narrower and moves towards its true position with the application of overlapping. **c)** As N_{ov} increases the measured velocity U converges towards the true velocity value at the center of a parabolic flow U_{center}.

3. Investigation of the image overlapping technique by synthetic images

Synthetic images of micro flows are used to investigate the effect of image overlapping on flow measurements. The number of the images is chosen so that a range of overlap numbers can be applied. Synthetic images were also generated with varying optical, particle and flow parameters to study the effects of these parameters. In summary the parameters under investigation are:

- Overlap number, N_{ov}
- Lens numerical aperture, NA
- Particle seeding density or number of particles per image, N_p
- Location of focal plane or local flow (either at the wall or center of a parabolic flow profile)

It is can be seen from equation (1) that the depth of correlation depends very weakly on lens magnification. For high magnification values, (M+1)/M approaches 1. Particle size also weakly affects the depth of the correlation especially for low NA lenses. In this section, the direct effect of lens magnification and particle size are not discussed. However, in reality, particle size can significantly affect signal-to-noise ratio.

From the measured velocity, it is also possible to estimate the effective depth of measurement and how it varies with the overlap number. This is done by mapping the measured velocity to the Gaussian filtered velocity profile.

Synthetic image generation and testing conditions

Synthetic images were generated by projecting random particles through a lens system onto a sensor array model. Lens of different magnifications, numerical apertures and therefore correlation depths were used: {M, NA, z_{corr}} = {05X, 0.12, 89.0μm}, {05X, 0.15, 58.2μm} and {10X, 0.3, 13.5μm}, where the depths of correlation of the system were calculated using equation (1). The particles were randomly generated inside a simulated 200μm deep and infinitely wide micro channel where the particle intensity is modeled as Gaussian profile (Olsen *et al* 2000). Two particle sizes, 2 and 1μm, were used with 5X and 10X lens respectively, to maintain the size of the in-focus particles in the image. The particles were displaced by a parabolic Poiseuille velocity profile as illustrated in Fig. 1. Shear gradients of 0.2 for 10X lens and 0.4 for 05X lens were used to maintain identical particle displacement at the center of the channel at the two different magnifications. The

number of particles throughout the volume of each image was chosen as 1250, 2500, 5000 and 10000. The image intensity was converted to 8-bit grayscale before saving into image files. A set of 2048 image pairs, 1024×1024 pixels in size, was generated for each case study. Noise was not added to the images. For fast image generation, particle intensity was calculated only within a radius equal to the particle effective diameter; this was found to have an insignificant effect on the final images. The particle effective diameter d_p at a z position is defined by Olsen and Adrian (2000):

$$d_e(z) = \left(M^2 d_p^2 + \frac{5.95(M+1)^2 \lambda^2}{4NA^2} + \frac{4M^2 z^2 NA^2 s_0^2}{(s_0+z)^2} \right) \tag{5}$$

where s_0 is lens working distance.

The overlap number was selected as an exponential series 2^i, where i=0, 1, 2.., 11. For i = 0, no image overlapping is performed, i.e. PIV processing is applied to each of the 2^{11} (2048) image pairs to produce corresponding correlation maps which are averaged to obtain a single correlation. For i = 11, all image pairs are overlapped to obtained one image pair and therefore one correlation map. For i = [1, 10], a combination of image overlapping and correlation averaging is performed so that all 2048 image pairs are used to produce one correlation map.

PIV processing was applied using a direct correlation function (without Fourier transform) and an image template size of 64x64 pixels. Prior to processing, background subtraction was applied to all image pairs. The standard deviation of the velocity measurements in all templates was calculated to verify that the all measurements are convergent.

Estimation of depth of measurement

For the synthetic data, the discrepancy between the measured and actual velocities can be used to estimate the depth of the measurement volume. The known velocity profile is convoluted with a Gaussian filter, with standard deviation σ_{filter}, centered on the focal plane as shown in Fig. 4a. The Gaussian filter represents the variation of particle correlation weight throughout the channel depth. The standard deviation of the filter is non-dimensionalised by the standard deviation of the particle correlation weighting function, to yield the non-dimensionalised depth of measurement z*.

$$z^* = \sigma_{filter}/\sigma_{corr} \tag{6a}$$

From equation (2) z^* is also equal to,

$$z^* = 3\sigma_{filter}/z_{corr} \tag{6b}$$

Similarly, we define the dimensional measurement depth z_{meas} such that:

$$z^* = z_{meas}/z_{corr} \tag{6c}$$

For a given optical setup σ_{corr} and z_{corr} are constants. As the width of the filter function is varied with corresponding changes in z*, the filtered velocity is changed, as shown in Fig. 4b for measurements at the center plane. When the measurement depth approaches zero, the filtered velocity approaches the velocity at the image focal plane. The variation of the filtered velocity with z*, Fig. 4b, is then mapped onto the variation of the velocity distribution with N_{ov}, Fig. 4c, to determine z* as a function of N_{ov}, Fig. 4d. The forms of Fig. 4b and 4c are specific to the location of the focal plane, in this case at the center of the channel. The exact form of the variation of the measurement depth with N_{ov} is also location dependent. However, within the limitation of the overlapping technique, increasing N_{ov} will always result in a decrease of the measurement depth.

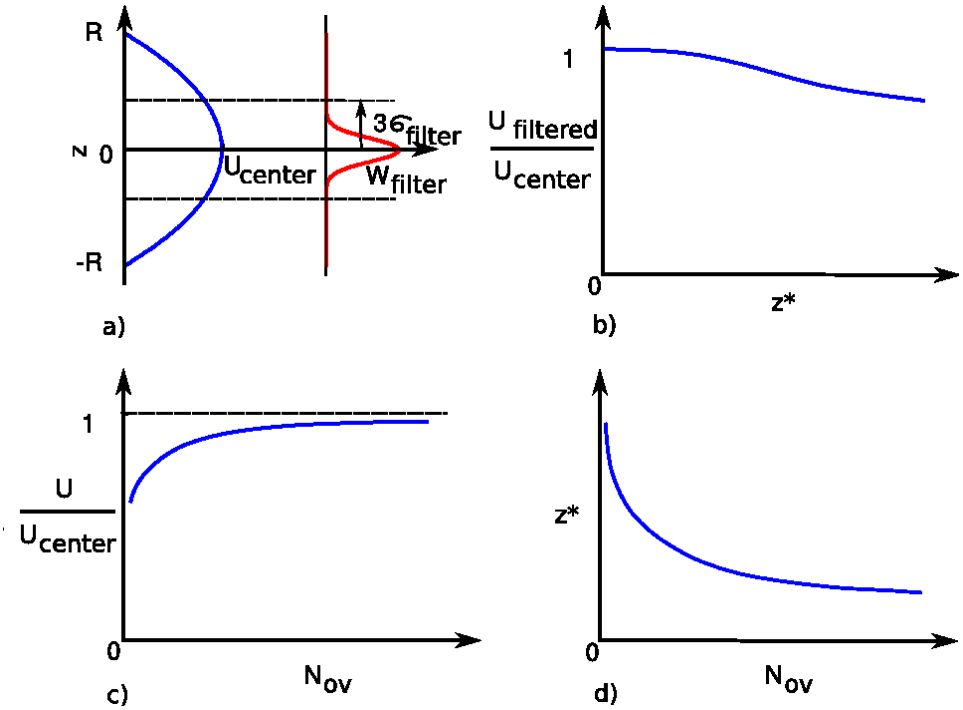

Fig. 4 A method to determine the depth of measurement as a function of overlap number, N_{ov}. The case illustrated is a parabolic velocity profile with the focal plane at the center of the profile. **a)** The velocity profile is filtered with a Gaussian weighting function W_{filter} with standard deviation σ_{filter}. **b)** Variation of the depth of measurement ($z^* = z_{meas}/z_{corr}$) alters the normalized filtered velocity as shown. **c)** Application of the overlap technique also changes the normalized measured velocity; the variation of the measured velocity at the center of the channel with N_{ov} is reproduced from Fig 3. **d)** By equating $U_{filtered}$ and U in b) and c) the variation of z* with N_{ov} is obtained. Increasing image overlapping results in decreasing depth of measurement.

4. Synthetic image results

In this section, the effect of image overlapping is studied using synthetic data. The flow studied is the parabolic channel flow described above. Specifically, we consider the flow properties at two locations: the focal plane at the center of the channel (where $U = U_{center}$) and the focal plane at the wall (where U = 0). The main benefit of this approach is that the actual velocity profile is known allowing validation of the technique. Figures 5b, 6b, 7b and 8b demonstrate the effect of N_{ov} on the normalized measurement depth z*, where $z^* = z_{meas}/z_{corr}$. In practical terms, it should be noted that both z_{corr} and z_{meas} are smaller at larger values of NA.

Performance of image overlapping with lenses of different numerical apertures

Fig. 5a shows the velocity measured with the focal plane at the center of the channel as the overlap number is varied for three different lenses. The particle density is held constant at 5000 particles per image. Note: the maximum value of $N_{ov} = 2048$ corresponds to the case where all images are overlapped. For all lenses, there is an initial rapid improvement in the measurement accuracy as N_{ov} increases from 1. As N_{ov} increases further the measured velocity converges more slowly towards the true value. The variation of the corresponding normalized depth of measurement z* is shown in Fig. 5b. As expected, z* decreases up to 3 times with increasing the overlap number. Clearly more accurate measurement results are obtained with lenses of higher numerical aperture. However, image overlapping produces significant improvement in measurement accuracy at lower NA values.

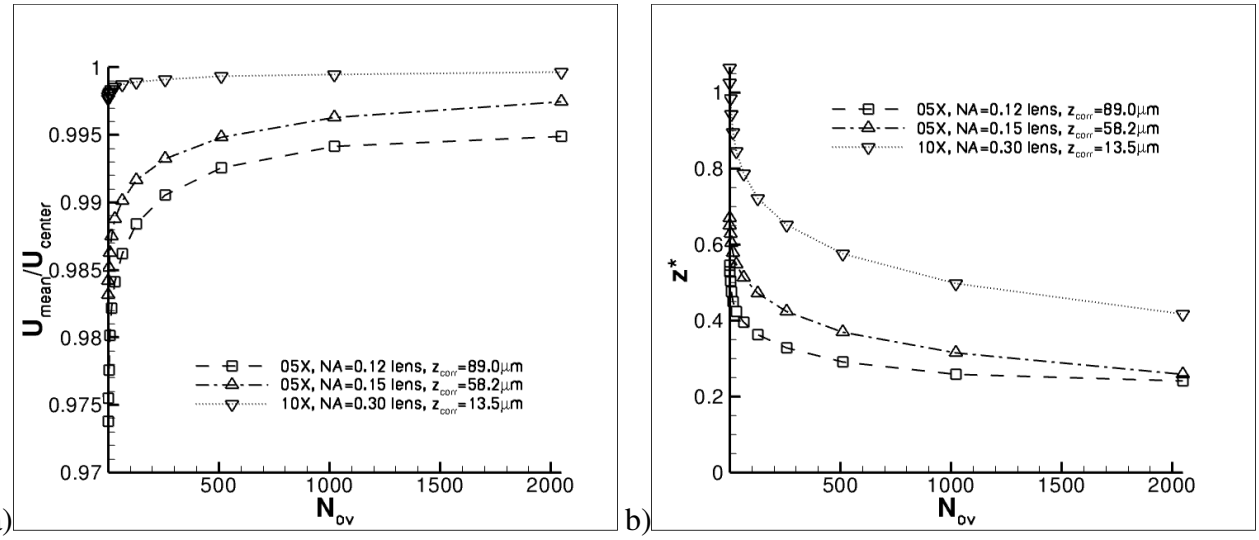

Fig. 5 Variation of **a)** measured velocity and **b)** depth of measurement with overlapping number for lenses with NA = 0.12, 0.15 and 0.30, (N_p = 5000 for all cases). The focal plane is at the centre of the channel. Increasing overlapping improves the measurement accuracy and reduces z* up to 3 times and higher NA lenses give improved accuracy.

In Fig. 6 the performance of overlapping with the three lenses is evaluated with the focal plane at the channel wall. In theory, the velocity measurements shown in Fig. 6a should be zero, however due to the motion of the out of focus particles the velocities are significantly over estimated, particularly without overlapping. Without image overlapping, the measurement using two 5X lenses produces spurious results with measured velocities close to 80% of the center velocity. As overlapping is applied the measured velocities converge towards zero with increasing overlap number. In this case image overlapping is able to produce accurate measurement values for the 5X lenses with low NA where previously the measurement would have failed. Fig. 6b shows the variation of z*. Interestingly with the same lens and particles the values of z* are smaller at the wall than at the flow center indicating that z* also depends on the local flow profile.

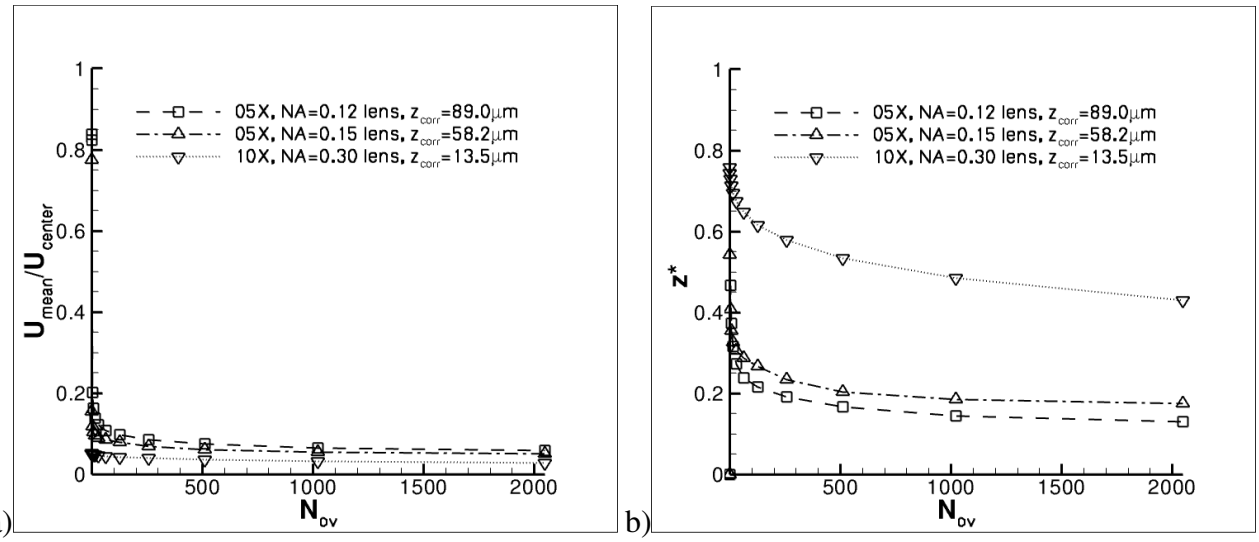

Fig. 6 Variation of **a)** measured velocity and **b)** depth of measurement with overlapping number for lenses with NA = 0.12, 0.15 and 0.30, (N_p = 5000 for all cases). The focal plane is at the channel wall. The measurement produces spurious results at NA = 0.12 and 0.15 when no image overlapping is applied.

Performance of image overlapping with different seeding concentrations:

Fig. 7 and 8 examine the effect of image overlapping with different seeding densities. The same lens (5X, NA = 0.15) is used for all cases. Without overlapping, the measured velocity and the depth of measurement only varies slightly with seeding density. As N_{ov} increases, the higher

seeding density produces better improvement in measurement accuracy. However, at maximum overlap and particle density (N_{ov} = 2048 and N_p = 10000) at the center of the channel, the image begins to become saturated with particles and Fig. 7 shows a decrease in the rate of improvement.

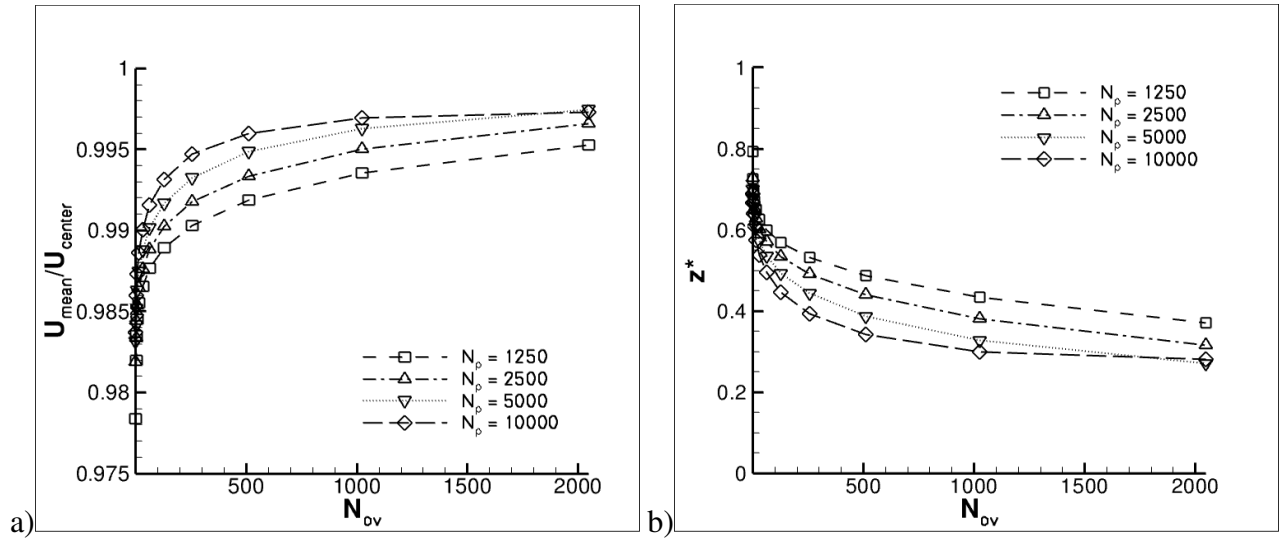

Fig. 7 Variation of **a)** measured velocity and **b)** depth of measurement with overlapping number for image particle densities of N_p = 1250, 2500, 5000 and 10,000. A 5X, NA = 0.15 lens was used for all cases and the focal plane is at the centre of the channel. Higher seeding density provides better measurement accuracy and smaller z*.

Fig. 8a and 8b show velocity and z* measurements at the wall. Again, the difference in z* between Fig. 7b and 8b again suggest that z* is dependent on the local flow profile.

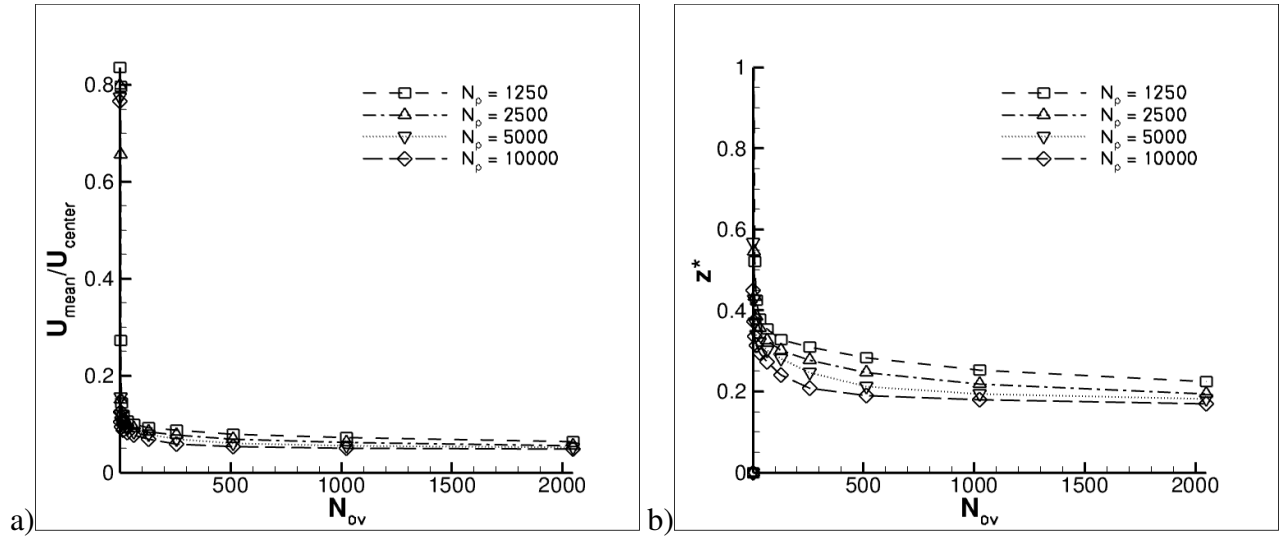

Fig. 8 Variation of **a)** measured velocity and **b)** depth of measurement with overlapping number for image particle densities of N_p = 1250, 2500, 5000 and 10,000. A 5X, NA = 0.15 lens was used for all cases and the focal plane is at the channel wall. The measurement produces spurious results at all seeding densities when no image overlapping is applied.

5. Application to experimental images

This section investigates the performance of image overlapping using experimental images. Scanning PIV is used to measure the velocity profile in a channel which can be compared to the theoretical profile. For the scanning technique, PIV data is acquired at each depth position to provide time-averaged velocity data in that plane allowing the extraction of the out-of-plane velocity profile. Experiments were carried out using 1 μm particles. The particle solution was prepared from 1 part of particles (5% solid suspension), 10 parts glycerine and 10 parts distilled

water by volume. The refractive index of particle solution was approximately 1.4. A 20X and NA=0.4 objective lens was used in conjunction with 0.7X tube lens. The particle solution was perfused through a micro channel of nominal cross-section $1000\times110\mu m^2$ with a constant flow rate of 0.18ml/min. The Reynolds number based on channel height was approximately 0.7, therefore the flow in the channel should be fully developed and the velocity profile parabolic.

The positions of the top and bottom walls (in the z direction) were identified using images of residual fluorescent particles on the walls of the empty channel. Scanning images were captured at different z positions and an auto-correlation applied to obtain a correlation peak distribution in the z direction. The auto-correlation peak is maximised at the walls and the exact wall positions are then estimated by curve fitting.

Scanning PIV was performed throughout the channel depth. At each z position, 20 image pairs were taken. The image pairs were then processed by 2 methods:

- Using correlation averaging only. Each image pair is cross correlated. Then correlations of image pairs are time-averaged.
- Using image overlapping only. The image pairs are overlapped into 1 image pair. This image pair is cross correlated.

For both techniques, the velocity was obtained from correlation map by 3 point Gaussian fit. Fig. 9 shows the velocity profiles obtained from both correlation averaging (as triangles) and image overlapping (as dots). The solid line was produced by parabolic fitting of the image overlapping measurements.

Image overlapping produces significant improvement in the velocity measurements and clearly the overlapped data fits well to the expected parabolic velocity profile. The velocities measured using correlation averaging alone are very asymmetric. This can be explained by the fact that the camera is located on the left hand side of the velocity profile as shown in Fig. 9. Therefore the signal-to-noise ratio is lower for the measurements on the far side of the channel as shown in Fig. 10. The measurement improvement on the right side provided by image overlapping therefore can be considered as an improvement to the signal-to-noise ratio.

The velocities measured at the wall in Fig. 9 are non-zero due to the distortion of the correlation peak by out-of-focus particles. With image overlapping, the measurement produces a measurement closer to expected velocity profile than with correlation averaging.

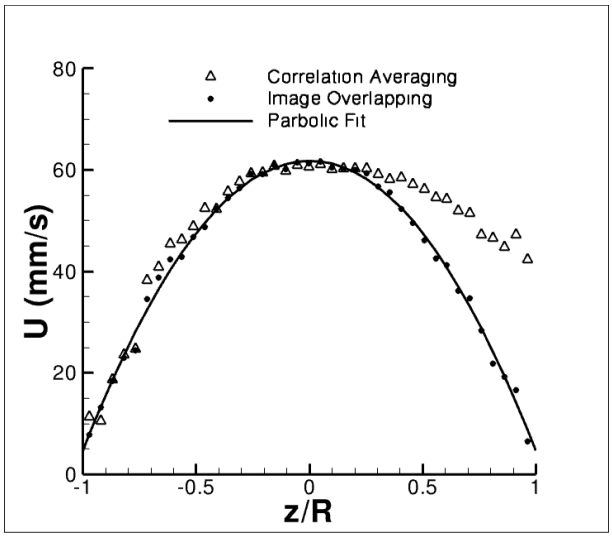

Fig. 9 Velocity profile measurements using correlation averaging (triangles) and image overlapping (dots) techniques on scanning PIV images using 1μm particles and N_{ov} = 20. The solid line is a parabolic fit of the measurement using image overlapping. The parabolic fit slightly overestimates the channel width. The difference between left part and right part of the measurement by correlation averaging is significantly. The camera is on the left side of the profiles. This figure shows that image overlapping can significantly improve signal-to-noise ratio on the far side of the channel.

The effect of image overlapping on the shape of correlation peaks at different z positions is illustrated in Fig. 10. Correlation maps, with and without overlapping, corresponding to the measurement data points in Fig. 9, are collated across the figures. Overlapping in Fig. 10a reduces the smearing of the peaks due out of focus particles as in Fig. 10b and increases signal-to-noise ratio on the right side of the figures.

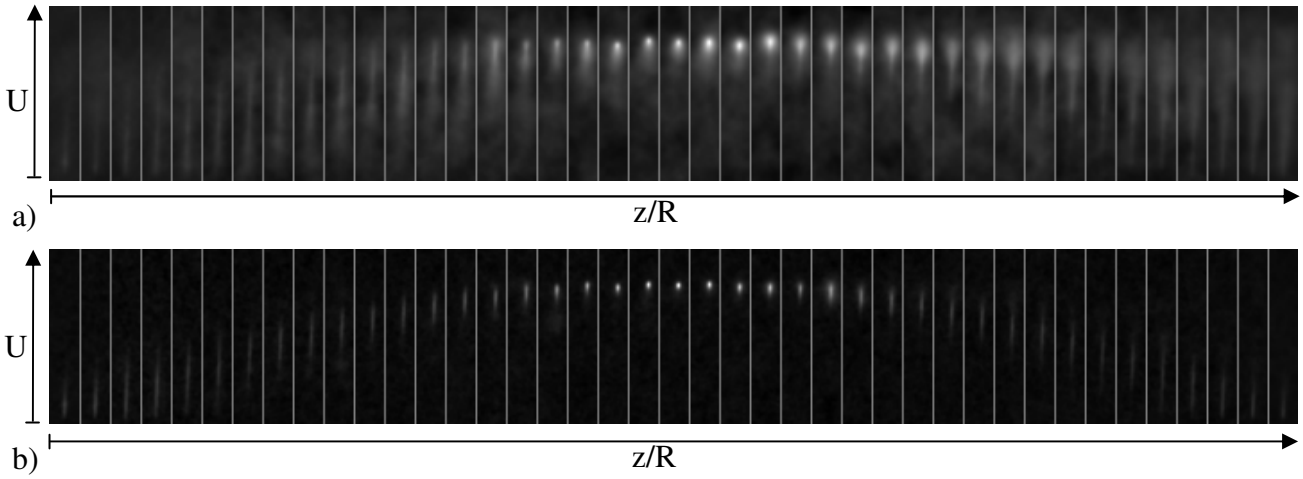

Fig. 10 Joined correlation maps side by side produced by **a)** correlation averaging technique and **b)** image overlapping technique. Each correlation map is 17×97 pixels and corresponds to a data point in Fig. 9. The bottom of the joined correlation maps is the zero velocity position for correlation peaks. Image overlapping effectively reduces blurring caused by out-of-focus particles and increase signal-to-noise ratio particularly in the far wall region.

6. Conclusions

A new important application of image overlapping improving the accuracy of micro PIV measurements has been demonstrated. The performance of image overlapping has been validated with both synthetic and experimental images of micro channel flows. The technique reduces the effective depth of measurement z* and increases signal-to-noise ratio, thereby increasing the measurement accuracy. The improvement obtained by image overlapping is significant even with a small overlap number. Importantly, the improvement is greatest near the channel wall. It was demonstrated for both synthetic and experimental data that under certain circumstances the application of image overlapping can produce accurate velocity measurement from previously unviable image data.

References

Bourdon CJ, Olsen MG, Gorby AD (2004) Power-filter technique for modifying depth of correlation in microPIV experiments. Experiments in Fluids 37(2), 263–271.

Bourdon CJ, Olsen MG, Gorby AD (2006) The Depth of Correlation in Micro-PIV for High Numerical Aperture and Immersion Objectives. Journal of Fluids Engineering 128, 883–886.

Meinhart CD, Wereley ST, Santiago JG (1999) PIV measurements of a microchannel flow. Experiments in Fluids 27(5), 414–419.

Olsen MG, Adrian RJ (2000) Out-of-focus effects on particle image visibility and correlation in microscopic particle image velocimetry. Experiments in Fluids 29(7), S166–S174.

Wereley ST, Gui L, Meinhart CD (2002) Advanced algorithms for microscale particle image velocimetry. AIAA Journal, 40, 1047–1055.

Wereley ST, Meinhart, CD, Gray MHB (1999) Depth effects in volume illuminated particle image velocimetry. In Third International Workshop on Particle Image Velocimetry Santa Barbara, CA, USA.